Available online at www.sciencedirect.com
ScienceDirect
Journal of Power Sources 172 (2007) 633–640
JOURNAL OF POWER SOURCES
www.elsevier.com/locate/jpowsour

Preparation and characterization of $Pr_{1-x}Sr_xFeO_3$ cathode material for intermediate temperature solid oxide fuel cells

Jinhua Piao, Kening Sun *, Naiqing Zhang, Xinbing Chen, Shen Xu, Derui Zhou

Department of Applied Chemistry, Harbin Institute of Technology, No. 92 West Dazhi Street, P.O. Box 211, Zip Code 150001 Harbin, PR China

Received 31 March 2007; received in revised form 10 May 2007; accepted 11 May 2007
Available online 18 May 2007

Abstract

A kind of cathode material of $Pr_{1-x}Sr_x$ FeO_3 ($x=0$–0.5) for intermediate temperature solid oxide fuel cells (IT-SOFCs) was prepared by the coprecipitation method. Crystal structure, thermal expansion, electrical conductivity and electrochemical performance of the $Pr_{1-x}Sr_xFeO_3$ perovskite oxide cathodes were studied by different methods. The results revealed that $Pr_{1-x}Sr_xFeO_3$ exhibited similar orthorhombic structure from $x=0.1$ to 0.3 and took cubic structure when $x=0.4$–0.5. The unit cell volume decreased and the thermal expansion coefficient (TEC) of the materials increased as the strontium content increased. When $0<x\leq 0.3$, the samples exhibited good thermal expansion compatibility with YSZ electrolyte. The electrical conductivity increased with the increasing of doped strontium content. When $x=0.3$–0.5, the electrical conductivities were higher than 100 S cm^{-1}. The conductivity of $Pr_{0.8}Sr_{0.2}FeO_3$ was 78 S cm^{-1} at 800 °C. Compared with the $La_{0.8}Sr_{0.2}MnO_3$ cathode, $Pr_{0.8}Sr_{0.2}FeO_3$ showed higher polarization current density and lower polarization resistance (0.2038 Ω cm^2). The value of I_0 for $Pr_{0.8}Sr_{0.2}FeO_3$ at 800 °C is 123.6 mA cm^{-2}. It is higher than that of $La_{0.8}Sr_{0.2}MnO_3$. Therefore, $Pr_{1-x}Sr_xFeO_3$ can be considered as a candidate cathode material for IT-SOFCs.

Keywords: $Pr_{1-x}Sr_x$ FeO_3; Cathode; Conductivity; Thermal expansion; Impedance spectra

1. Introduction

For solid oxide fuel cells (SOFC) cathodes, the selected materials must have superior catalytic activity, chemical and structural stability and compatibility with adjacent cell components, not only under operation conditions, but also at high temperatures where the membranes are fabricated [1–3]. The lanthanum manganite-based perovskite oxides, such as $La_{1-x}Sr_xMnO_3$ (particularly, $x=0.1$–0.3), have been used extensively as the cathode material for SOFC [4–7]. However, the lanthanum strontium manganite perovskite oxide has some disadvantages, for example, low ionic conductivity. Particularly, the low oxide ion conductivity product of the pyrochlore oxide $La_2Zr_2O_7$ is formed at the boundary with the yttria-stabilized zirconia (YSZ) electrolyte when the annealing temperature is above 1200 °C [5]. Strontium-doped lanthanum cobaltile/ferrites-based oxides possess excellent mixed-conduction characteristics, relatively high ionic conductivity and high catalytic activity for oxygen reduction [8,9]. Nevertheless, Strontium-doped lanthanum cobaltile-based oxide exhibits high thermal expansion coefficient (TEC) and detrimental reaction with traditional stabilized zirconia electrolyte [10]. The perovskite compositions with Co, Ni, and Mn B-site cations indicated poor chemical, long-term performance stability and lower power densities than Fe as B-site cation [11,12]. Sakaki et al. reported that better catalytic activity can be achieved by replacing lanthanum with heavier earth metal in A-site of the $LnMnO_3$ (Ln = Pr, Nd, Sm, Eu, Gd) material, which can also hamper the reaction between the cathode and electrolyte [5]. Therefore, better stability and performance of cathodes can be expected by replacing La with Pr in A-site and replacing Mn with Fe in B-site of the composition.

Structure and magnetism of $Pr_{1-x}Sr_xFeO_{3-\sigma}$ (PSF) were reported by H.W. Brinks [13]. However there is no systematic report about praseodymium ferrite as cathode material for SOFCs. In this work, the $Pr_{1-x}Sr_xFeO_3$ ($x=0$–0.5) perovskite oxide cathodes were studied as a novel cathode material for SOFCs. The crystal structure, electrical conductivity, thermal expansion compatibility, reactivity with YSZ electrolyte and the electrochemical performance were studied.

* Corresponding author. Tel.: +86 451 86412153; fax: +86 451 86412153.
E-mail address: sunkn@hit.edu.cn (K. Sun).

0378-7753/$ – see front matter © 2007 Elsevier B.V. All rights reserved.
doi:10.1016/j.jpowsour.2007.05.023

2. Experimental

Small batches of perovskite powders comprising a range of compositions described by $Pr_{1-x}Sr_xFeO_3$ ($x = 0$–0.5) and $La_{0.8}Sr_{0.2}MnO_3$ (LSM20) were prepared as the cathode materials for SOFCs. For this purpose, precursors were synthesized by the coprecipitation method. Stoichoimetric amount of $Pr(NO_3)_3{\cdot}6H_2O$, $Mn(NO_3)_2{\cdot}6H_2O$, $Fe(NO_3)_3{\cdot}9H_2O$, $La(NO_3)_2{\cdot}6H_2O$ and $Sr(NO_3)_2$ (all with a purity level of >99.9%, Gansu Rare Earth) were dissolved into water and then titrated into $NH_4HCO_3/NH_3{\cdot}H_2O$ (pH = 10.0) buffer solution which was stirred constantly. After washed by deionised water, the precursors were subsequently heated at 1000 °C for 2 h to obtain the powders. The milled powder was made into rod by being uniaxially pressed under a pressure of 25 MPa and then sintered at 1200 °C for 6 h for measuring thermal expansion coefficient. The dimension was approximately 2 mm × 5 mm × 12 mm.

The crystal structures of the synthesized powders were characterized with Rigaku D/max-∏B X-ray diffractometer (XRD) using Cu Kα radiation. The electrical conductivities were measured with temperature range from 400 to 900 °C by the four-probe dc method. The electrical conductivities were measured using Keithley 2400 sourcemeter. The thermal expansion coefficients (TEC) were obtained in air with a Netzsch dilatometer. Samples were heated at a rate of 10 °C min^{-1} up to 1000 °C.

In order to study the reactivity of $Pr_{1-x}Sr_xFeO_3$ cathodes with YSZ (Tosoh, Japan) electrolyte, the $Pr_{0.8}Sr_{0.2}FeO_3$ cathode and YSZ electrolyte powders were mixed in a weight ratio of 1:1, pressed into pellet under an uniaxial pressure of 25 MPa, heated at 1200 °C for 6 h and then at 800 °C for 100 h. The reaction product was detected using XRD.

A YSZ electrolyte pellet was prepared by being sintered at 1550 °C for 6 h with the size of 15 mm in diameter and 0.6 mm in thickness. Three-electrode set-up was used to measure the electrochemical performance. The powders of $Pr_{1-x}Sr_xFeO_3$ ($x = 0.1$–0.5) were made into slurry by being mixed with ethylcellulose binder and organic solvent (terpineol). The slurry was screen-printed onto one side of the electrolyte pellet before being sintered at 1200 °C for 2 h to prepare cathode (WE). The cathode area was 0.25 cm^2. A commercial Pt paste (PC-Pt-7840, Sino-Platinum Metals) was painted on the cathode side as reference electrode (RE) and painted to the other side of the electrolyte pellet as the counter electrode (CE) (Fig. 1). The counter area was 0.49 cm^2. The Pt electrodes were fired at 850 °C for 30 min. The electrochemical performance of the cells was measured using a potentiostat/galvanostat (model PARSTAT® 2273, Princeton Applied Research). The impedance frequency range was 10 mHz to 10^5 Hz with a signal amplitude of 5 mV. The impedance fitting analysis was controlled with software (Zsimpwin).

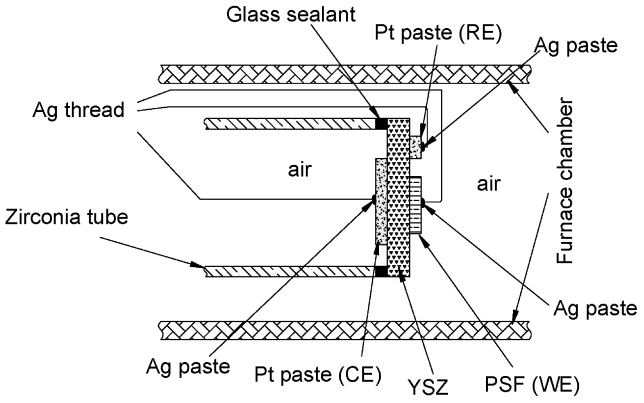

Fig. 1. Holder of three-electrode setup for high temperature electrochemistry measurement.

3. Result and discussion

3.1. Crystal structure

In Fig. 2a, the XRD patterns of $Pr_{1-x}Sr_xFe0_3$ ($x = 0.1$–0.5) (PSF) are given. The X-ray diffraction results (checked by XRD phase analysis software) showed that all the prepared $Pr_{1-x}Sr_xFeO_3$ ($x = 0.1$–0.5) were single phase perovskite solid solutions without detectable impurity phases. In this work, the structure of the compounds with $x \leq 0.3$ was the orthorhombic $GdFeO_3$-type structure (*Pbnm* space group), which is a distorted perovskite structure. Each unit cell consists of four units, and has

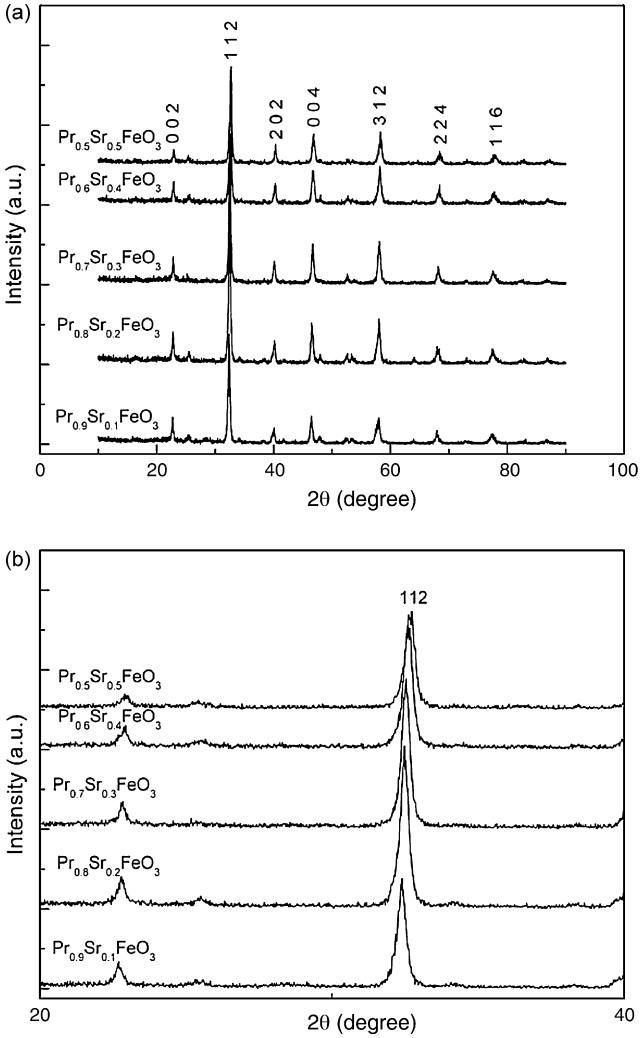

Fig. 2. XRD patterns for $Pr_{1-x}Sr_xFeO_3$ ($x = 0.1$–0.5).

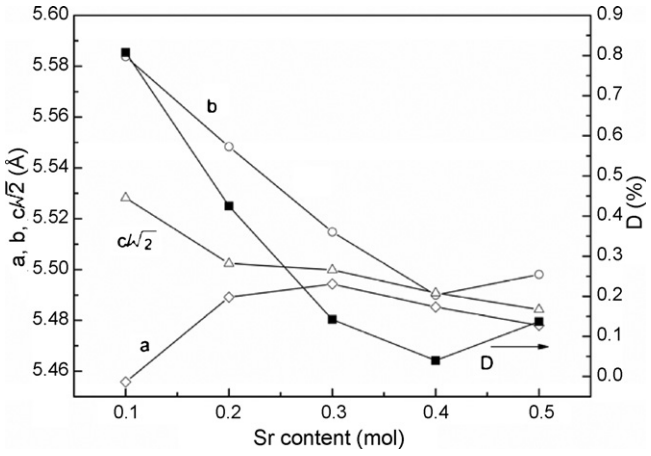

Fig. 3. Lattice parameters (*Pbnm* model) (a, b, c, $\sqrt{2}$) and orthorhombic deformation D (%) of $Pr_{1-x}Sr_xFeO_3$ as a function of Sr content.

the approximate dimensions $\sqrt{2}a_p \times \sqrt{2}a_p \times 2a_p$, where a_p is the lattice parameter of the ideal cubic unit cell. For $x = 0.4$ and 0.5, cubic structure (space group *Pm-3m*) was determined as the approximation of the true structure (agreed with the report of Brinks [13]). From Fig. 2b, it can be found that the peak (1 1 2) position slightly shifted as the strontium content changed from 0.1 to 0.5. The unit-cell dimensions (*Pbnm* model) for $Pr_{1-x}Sr_xFeO_3$ as a function of the composition parameter x were shown in Fig. 3 and Table 1. The cell volume decreased with the increasing of Sr content. In $Pr_{1-x}Sr_xFeO_3$, the substitution of a large Sr^{2+} ion (1.44 Å) for a small Pr^{3+} ion (1.30 Å) [14] will result in a larger volume. At the meanwhile, the heterovalent substitution will induce the increase of Fe valence. The smaller size of Fe^{4+} compared with Fe^{3+} will lead to a smaller volume consequently. In $Pr_{1-x}Sr_xFeO_3$, the effect on volume change brought by the substitution of Fe^{3+} for Fe^{4+} was more significant than that arouse from the Sr^{2+} replacement of Pr^{3+} [13]. Therefore, the volume decreased as the Sr content increased.

In $PrFeO_3$ perovskite structure, the small Pr^{3+}ion located at the center of the cubic. As a result, the FeO_6 octahedra are tilted and rotated to fill the extra space around the Pr^{3+} cation, causing the distortion. The Goldschmidt tolerance factor t can be used as a measure of the deviation of the ABO_3 perovskite structure from the ideal cubic symmetry, [1]

$$t = \frac{r_A + r_o}{\sqrt{2}(r_B + r_o)} \quad (1)$$

where r_A, r_B, and r_o are the radii of A^{3+}, B^{3+}, and O^{2-} ions, respectively. The tolerance factor for $PrFeO_3$ can be calculated as $t = 0.93$, (the ionic radii of 1.30 Å for Pr^{3+}, 0.645 Å for Fe^{3+}, 1.40 Å for O^{2-}) [14]. Here Fe is in the trivalent state. Actually, some tetravalent Fe ions will exist as large size of Sr^{2+} is introduced at Pr^{3+} lattice positions because of electronic charge compensation. Value t will increase because the facts that the size of Sr^{2+} is larger than that of Pr^{3+} and the size of Fe^{4+} is smaller than that of Fe^{3+}. So the crystal structure was closer to ideality.

In addition, the orthorhombic deformation (D) quantitatively expresses the macroscopic distortion relative to the ideal perovskite structure. D defined as [15]:

$$D = \frac{1}{3}\sum_{i=1}^{3}\left|\frac{a_i - \bar{a}}{\bar{a}}\right| \times 100 \quad (2)$$

where $a_i = a$, $a_2 = b$, $a_3 = c/\sqrt{2}$, and $\bar{a} = (abc/\sqrt{2})^{1/3}$.The values of D, calculated for each compound, are shown in Fig. 3 and Table 1. As can be found, the D value of $x = 0.1$ was the highest because of the high value of the parameter b. The increase of Sr content results in the decrease of D, which reaches smallest value at $x = 0.4$. The D value increases again when $x = 0.5$ because of the deviation of the lattice parameters.

In order to illustrate the effect of Sr content on the size of the unit cell, the pseudocubic lattice parameter, a', is defined as the cubic root of the unit cell volume per ABO_3 unit:

$$a' = (V/z)^{1/3} \quad (3)$$

where $z = 4$ for the oxides of this study. The values of a' is shown in Fig. 4. As can be seen, a' decreases with increasing Sr content as a result of the oxidation of Fe^{3+} to the smaller Fe^{4+} cation. Another factor is that the formation of the tetravalent Fe ions is expected to strengthen the Fe–O bonds in FeO_6 octahedra according to Pauling's second rule. As a result, the size FeO_6 octahedra and the volume of the perovskite unit cell decrease.

3.2. Conductivity

The effect of Sr content on the electrical conductivities for $Pr_{1-x}Sr_xFeO_3$ ($x = 0$–0.5) was investigated. The dependence of electronic conductivity on temperature was shown in Fig. 5. As strontium content increases, the electrical conductivity of $Pr_{1-x}Sr_xFeO_3$ increases. The electrical conductivity was all higher than 100 S cm^{-1} when $x = 0.3$–0.5. And $Pr_{0.5}Sr_{0.5}FeO_3$ has a maximum conductivity of 300 S cm^{-1} at 550 °C. The electrical conductivity of $Pr_{0.8}Sr_{0.2}FeO_3$ is 78 S cm^{-1} at 800 °C. It meets the requirement of SOFC cathode. For $La_{1-x}Sr_xFeO_3$ (LSF), similar trend were showed. The highest conductivity,

Table 1
Lattice parameters (*Pbnm* model) (a, b, c, $\sqrt{2}$) and orthorhmbic deformation for $Pr_{1-x}Sr_xFeO_3$

x	a (Å)	b (Å)	c (Å)	volume (Å^3)	$c/\sqrt{2}$ (Å)	Orthorhombic deformation D (%)
0.1	5.45576	5.58375	7.81689	238.13	5.5282	0.8053
0.2	5.48914	5.54835	7.7804	236.96	5.5024	0.425
0.3	5.49431	5.51483	7.77684	235.64	5.4999	0.142
0.4	5.4853	5.4900	7.7640	233.81	5.4908	0.04
0.5	5.47799	5.49808	7.75481	233.56	5.4843	0.137

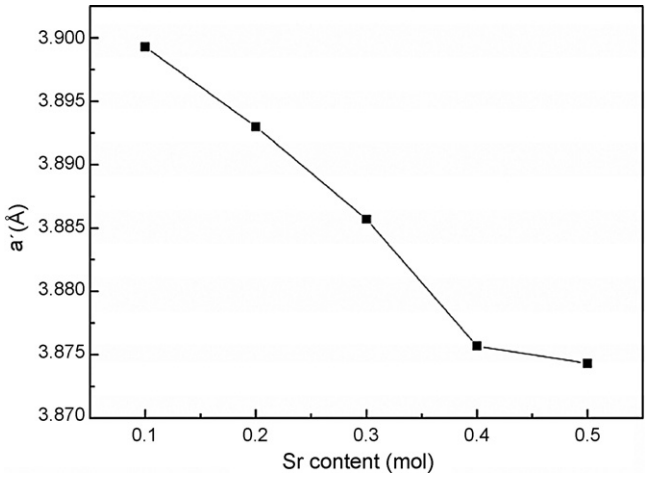

Fig. 4. Pseudo-cubic lattice constant (a') of $Pr_{1-x}Sr_xFeO_3$ as a function of Sr content.

352 S cm^{-1}, was found at 550 °C for a composition of $x = 0.5$. The conductivity of $La_{0.8}Sr_{0.2}FeO_3$ is similar to $Pr_{0.8}Sr_{0.2}FeO_3$ which is lower than 100 S cm^{-1} [16]. In $Pr_{1-x}Sr_xFeO_3$ perovskites, substitution of a divalent cation (Sr) for a trivalent cation (Pr) results in the oxidation of Fe^{3+} cations to Fe^{4+} for charge compensation. As the strontium content increases, the Fe^{4+} charge carriers content increases linearly when $x < 0.5$ (proved by Brinks [13]) and higher electrical conductivity can be achieved. It is also evident that the electrical conductivity of $Pr_{1-x}Sr_xFeO_3$ ($x > 0.3$) decreases when temperature goes higher. The decreasing trend of electrical conductivity became more obvious when the doped strontium content increases because the oxygen deficiency is enhanced at high temperature with x values increasing. The trend for LSF is same. The conductivity of $La_{0.5}Sr_{0.5}FeO_3$ decreases when temperature goes higher and it will be lower than 100 S cm^{-1} at 1000 °C [16]. The decrease is contributed to the fact that formation of significant amount of oxide ion vacancies which were accompanied by reduction of Fe^{4+} to Fe^{3+} at high temperature. It results in a decrease in the charge carrier concentration [13]. Therefore, the electronic conductivity decreases.

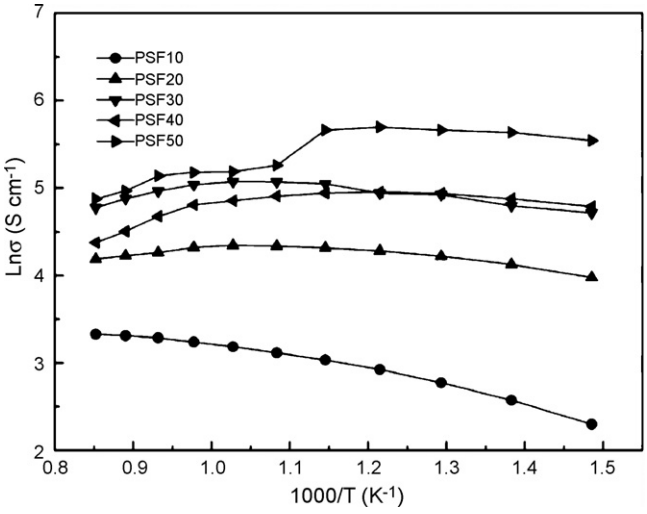

Fig. 5. Temperature dependence of the electrical conductivity for $Pr_{1-x}Sr_xFeO_3$.

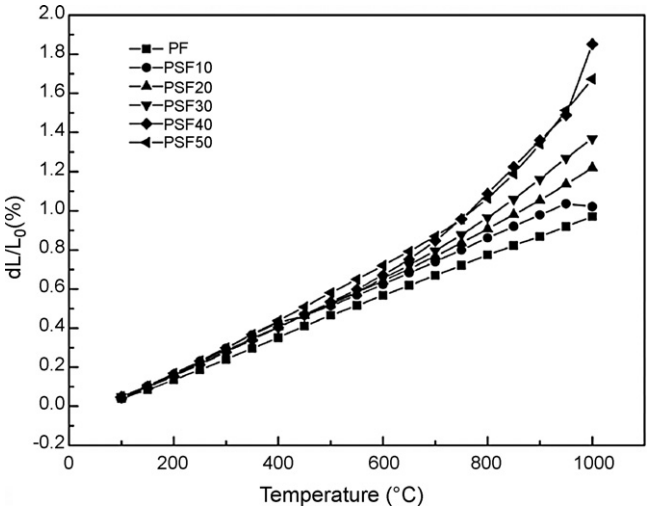

Fig. 6. Linear thermal expansion curves for $Pr_{1-x}Sr_xFeO_3$ as a function of temperature.

3.3. Thermal expansion

The thermal expansion curves of $Pr_{1-x}Sr_xFeO_3$ ($x = 0$–0.5) were shown in Fig. 6. For the electrode fabrication process, the adoption of the co-firing process of the electrolyte and electrode is vital. TEC match between electrolyte and electrode is very important. The thermal expansion depends on the electrostatic attraction forces within the lattice [17] and was affected evidently by the concentration of oxygen vacancy in $Ln_{1-x}Sr_xMO_3$ perovskite oxides. It can be found from Fig. 6 that the thermal expansion coefficients increased as the strontium content raise and the thermal expansion curves are nearly linear. For $x = 0.4$ and 0.5, the curves are linear only when the temperature is lower than 600 °C and they become steeper at high temperatures. This can be explained by the fact that the electrostatic attraction decreases when the strontium substitutes praseodymium. The electronegativity of Pr^{3+} (1.1) is larger than that of Sr^{2+} (1.0), which results in the increasing TEC when Sr^{2+} content increases from 10 to 50 mol%. Additionally, the variations of TEC are also related to the defect structures of $Pr_{1-x}Sr_xFeO_3$, which depend on the different strontium content and temperature. As the temperature increases, more oxygen vacancy and less Fe^{4+} formed. The content of Fe^{3+}, which possesses a larger ionic radius and weaker electrostatic attraction forces than Fe^{4+}, increases while the content of Fe^{4+} decreases. In addition, the reduction of the Fe^{4+} cation causes a decrease in the Fe–O bond strength according to Pauling's second rule, and hence the size of BO_6 octahedra increases, thus enhancing the lattice expansion. Oxygen deficiency is also enhanced at high temperature. Thus the TEC increases quickly at high temperature. The thermal expansion coefficients of $Pr_{1-x}Sr_xFeO_3$ for $x = 0.1$–0.3 match well with YSZ (10.8×10^{-6} K^{-1}, measured by our lab.) electrolyte. The TEC of PSF20 (12.1×10^{-6} K^{-1}) was similar to the TEC of LSF20 (12.0×10^{-6} K^{-1} [18]). The reason is that Pr^{3+} and La^{3+} have the same electronegativity value (1.1).

3.4. Impedance analysis for $Pr_{1-x}Sr_xFeO_3$ cathodes

The electrochemical performance is an important property of cathode for SOFCs. In this study, the cathode polarization resistance (R_p) and polarization current density of $Pr_{1-x}Sr_xFeO_3$ ($x = 0.1$–0.5) and $La_{0.8}Sr_{0.2}MnO_3$ have been measured at 800 °C. The complex impedance spectra were given in Fig. 7. Fits to these data show that the complex impedance plots are all composed of two arcs from $x = 0.1$ and 0.5. It shows that the oxygen reduction reaction is at least limited by two electrode processes during molecular oxygen reduction. The equivalent circuit $LR_s(QR_{ct})(CR_d)$ was showed in Fig. 7. L is attributed to high-frequency artifacts arising from the measurement apparatus. R_s is the ohmic resistance of electrolyte and lead wires (note that this part is not shown in the present data) [19]. The high-frequency arc is ascribed to charge-transfer resistance (R_{ct}) from the electrode/YSZ interface into the YSZ electrolyte and the low-frequency arc to the diffusion resistance (R_d) [17,20]. R_p includes the R_{ct} and R_d. It can be found that compared with the traditional $La_{0.8}Sr_{0.2}MnO_3$ cathode, the samples ($x = 0.1$–0.3) possess lower R_p values and the lowest R_p value achieved for $Pr_{0.8}Sr_{0.2}FeO_3$. The R_p value of $Pr_{0.8}Sr_{0.2}FeO_3$ cathode at 800 °C is 0.2038 Ω cm^2. Fig. 8 also shows that $Pr_{0.8}Sr_{0.2}FeO_3$ possessed optimum polarization current density and was better than that of $La_{0.8}Sr_{0.2}MnO_3$. This can be explained that $Pr_{0.8}Sr_{0.2}FeO_3$ possessed the lowest oxygen ion transfer resistance between electrode and electrolyte (Fig. 9). Although the conductivities of $Pr_{1-x}Sr_xFeO_3$ (x from 0.3 to 0.5) are higher than $Pr_{0.8}Sr_{0.2}FeO_3$, the role of oxygen ion transfer resistance between electrode and electrolyte was more significant than the role of the cathode conductivity in the electrode electrochemical performance.

Fig. 10showed the impedance spectra plots and the fitting curves for the $Pr_{0.8}Sr_{0.2}FeO_3$ cathode at different temperatures. For $Pr_{0.8}Sr_{0.2}FeO_3$, the high-frequency arc is larger than the low-frequency arc from 750 to 850 °C, which indicates

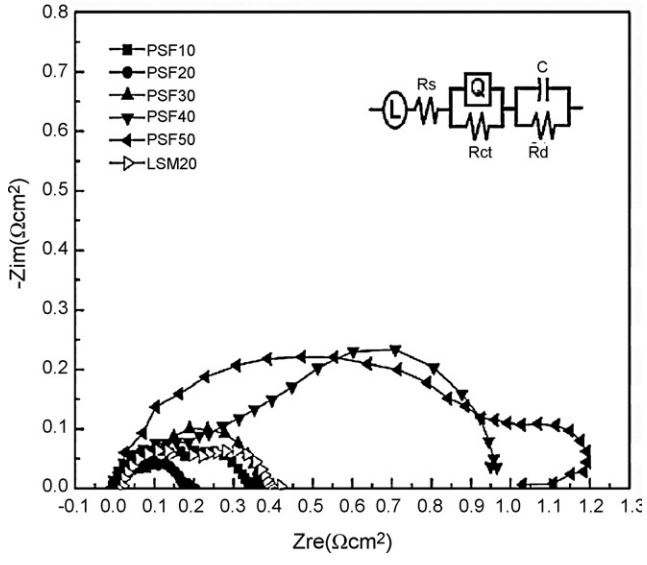

Fig. 7. The cathodic complex impedance plots of $Pr_{1-x}Sr_xFeO_3$ and $La_{0.8}Sr_{0.2}MnO_3$ at 800 °C in air.

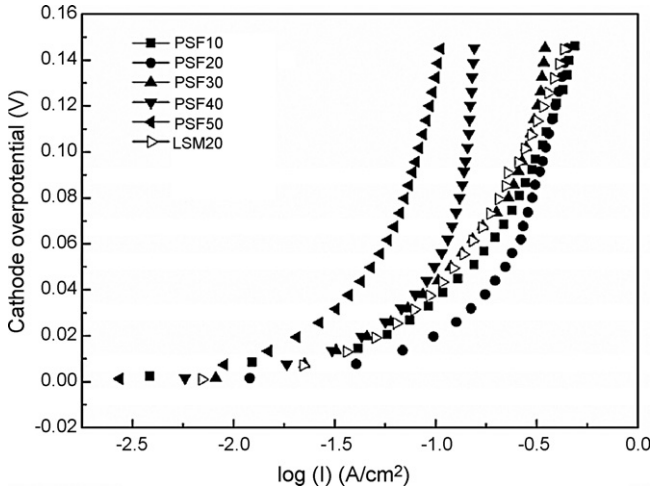

Fig. 8. Cathodic polarization curves for $Pr_{1-x}Sr_xFeO_3$ and $La_{0.8}Sr_{0.2}MnO_3$ at 800 °C.

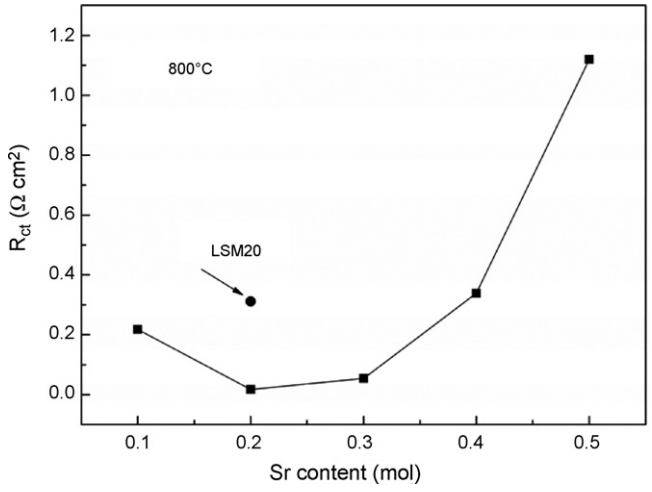

Fig. 9. Charge-transfer resistance between electrode and electrolyte as a function of Sr content.

charge-transfer processes probably limit the electrode reaction. As the temperature increase, both R_s and R_{ct} values of $Pr_{0.8}Sr_{0.2}FeO_3$ decrease significantly (as shown in Table 2) and the sizes of high-frequency arc (QR_{ct}) and low-frequency arc are decreased gradually. It also showed that the diffusion resistance R_d was similar at 800 and 850 °C. The high-frequency arc is larger than the low-frequency arc from 750 to 850 °C, which typically indicates that the charge-transfer processes is the rate-limiting step in the cathode reaction. These results showed that under cathodic polarization the kinetic processes of the oxygen reduction are not only controlled by charge-transfer but

Table 2
Parameters obtained by fitting ac impedance curves for PSF20 at different temperature

T (°C)	R_s (Ω cm^2)	R_{ct} (Ω cm^2)	R_d (Ω cm^2)	R_p (Ω cm^2)
750	1.865	0.6737	0.2124	0.8861
800	0.7441	0.1871	0.0167	0.2038
850	0.5538	0.1428	0.02097	0.1638

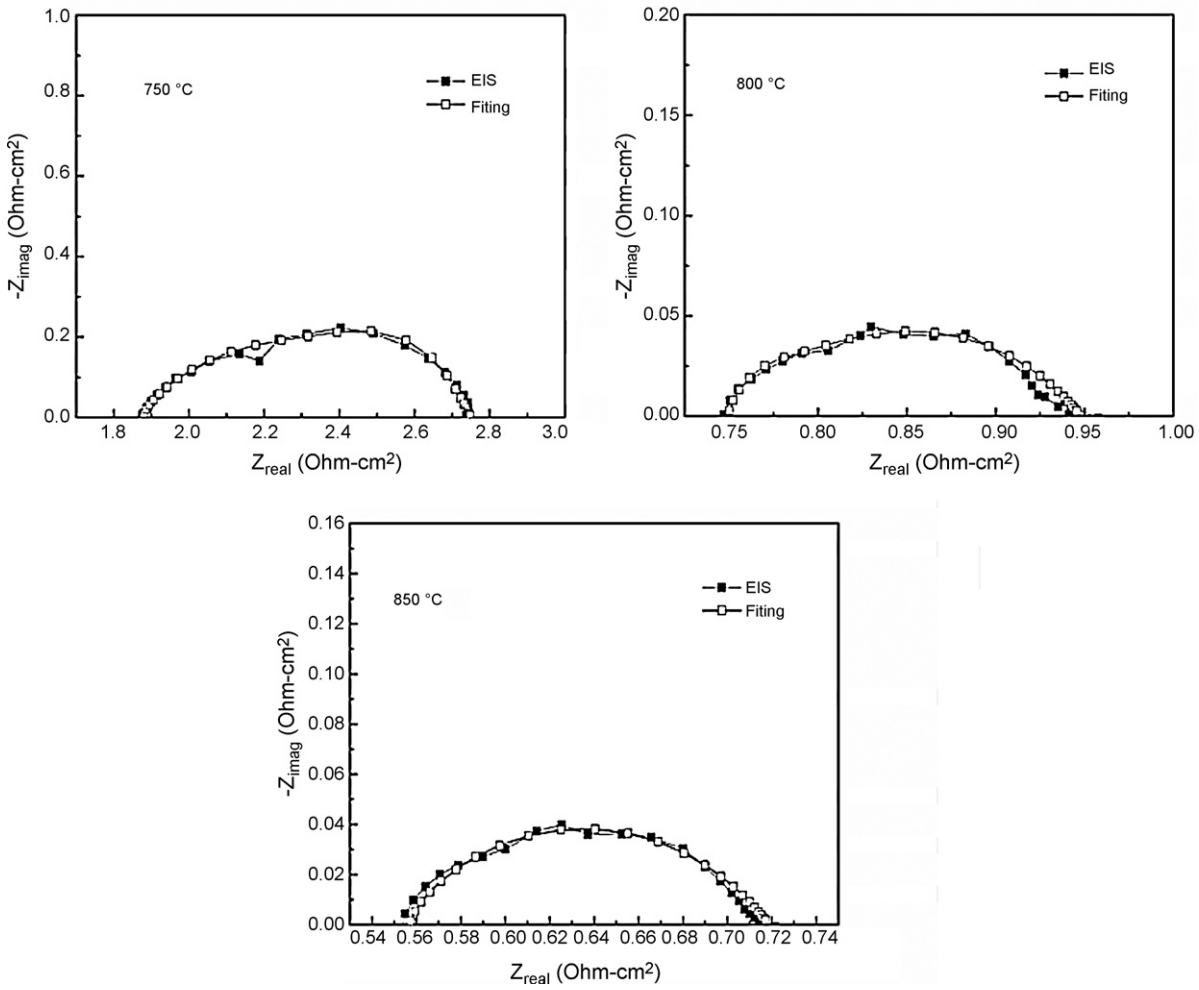

Fig. 10. Impedance spectra measured under open circuit condition at different temperature in air for $Pr_{1-x}Sr_xFeO_3$ cathodes.

also by adsorption/desorption and diffusion of oxygen. This corresponds to the fact that the oxygen reduction reaction is achieved through reaction steps such as adsorption, dissociation, diffusion, and charge transfer [21]. In the present study, the $Pr_{0.8}Sr_{0.2}FeO_3$ cathode displays a R_p value of 0.1638 Ω cm^2 at 850 °C, 0.2038 Ω cm^2 at 800 °C and 0.8861 Ω cm^2 at 750 °C Perry Murray and Barnett reported that the polarization resistance of $La_{0.8}Sr_{0.2}MnO_3$ cathode was 3.15 Ω cm^2 at 750 °C under open circuit on YSZ electrolyte substrates [19]. It is apparent that the $Pr_{0.8}Sr_{0.2}FeO_3$ cathode possessed better performance than $La_{0.8}Sr_{0.2}MnO_3$.

The total oxygen reduction reaction (ORR) requires the presence of gaseous oxygen and good electronic conductivity in the electrode material as well as the possibility for created oxide ions to be transported away from the reaction site into the bulk of the electrolyte [22]. The triple phase boundary (TPB) between electrode, electrolyte and gas phase in the bulk of the electrode can meet the requirements. Hence, it is conceivable that the polarization resistance of the optimized composite electrode is decreased by extending the length of TPB, which results in much lower overpotential toward oxygen reduction, and by increasing the oxygen diffusion upon addition of an ionic conducting phase (electrolyte). Perry Murray and Barnett compared the performance of the LSM–GDC ($Ce_{0.8}Gd_{0.2}O_{2-\delta}$) and LSM–YSZ composite cathodes with the pure LSM cathode. Their research showed that the composite cathode possessed better performance than pure electrode material. The R_p value of the LSM–GDC50 composite cathode was 0.49 Ω cm^2 and that of LSM–YSZ50 composite cathode was 1.31 Ω cm^2 at 750 °C. The R_p value of the pure LSM was the highest (3.5 Ω cm^2) [19]. Thus the performance for PSF–GDC and PSF–YSZ composite cathodes are to be studied in the next step work.

3.5. Determination the exchange current density (I_0) of the $Pr_{0.8}Sr_{0.2}FeO_3$

The exchange current density, I_0, can be calculated from the charge-transfer resistance R_{ct} (obtained from the fitting data of electrochemical impedance spectroscopy) according to the Eq. (4). The Eq. (4) is derived from the low current density regime approximation to the Bulter–Volmer equation is [20,23]:

$$I_0 = RT/nFR_{ct} \quad (4)$$

where n is the number of electrons which contribute the charge transfer reaction; R is the gas constant; F is the Faraday constant

and T is the absolute temperature. For the oxygen reduction reaction, n is assumed to be 4.

Values of I_0 for $Pr_{0.8}Sr_{0.2}FeO_3$ at different temperature and $La_{0.8}Sr_{0.2}MnO_3$ at 800 °C obtained from Eq. (4). The I_0 values of $Pr_{0.8}Sr_{0.2}FeO_3$ increases from 34.3 mA cm^{-2} at 750 °C to 161.9 mA cm^{-2} at 850°C. The value of I_0 for $Pr_{0.8}Sr_{0.2}FeO_3$ at 800°C is 123.6 mA cm^{-2}, which is higher than that of $La_{0.8}Sr_{0.2}MnO_3$ (74.3 mA cm^{-2}, measured by ourself). The values of I_0 for $Pr_{0.8}Sr_{0.2}FeO_3$ at different temperature are also higher than those of $Pr_{0.55}Sr_{0.4}MnO_3$ cathode (only 2.80 mA cm^{-2} at 750 °C and 4.69 mA cm^{-2} at 850 °C) [24]. These results suggest that the electrocatalytic activity of the $Pr_{0.8}Sr_{0.2}FeO_3$ is higher than that of the $La_{0.8}Sr_{0.2}MnO_3$. These results also suggest that the electrocatalytic activity of ferrites-based oxides is higher than manganite-based oxide when the A-site element is the same. The reason is that substitution of a divalent cation (Sr) for a trivalent cation in A-site results in the excellent mixed-conduction characteristics and relatively high ionic conductivity by the creation of more oxygen vacancies in ferrites-based perovskite oxides [8,9]. The oxygen vacancies on the electrode surface provide the reaction site for the reduction of the molecular oxygen and provide the pass way for the diffusion of the reduced oxygen ions [25,26]. Therefore, as a mixed ionic-electronic conductor (MIEC), $Pr_{0.8}Sr_{0.2}FeO_3$ improved the diffusivity of the oxygen ions from electrode surface to TPB. In other words, the ORR occurs at the air/PSF20 interface, as well as at the air/PSF20/YSZ triple phase boundary, while in the case of LSM, only the air/LSM/YSZ triple phase boundaries are active. It is apparent that the reason $Pr_{0.8}Sr_{0.2}FeO_3$ cathode has better performance than $La_{0.8}Sr_{0.2}MnO_3$ is that $Pr_{0.8}Sr_{0.2}FeO_3$ has larger oxygen ionic conductivity.

3.6. Reaction test

Fig. 11shows the XRD pattern of the PSF20–YSZ mixture, heated at 1200°C for 6 h and then at 800 °C for 100 h. It can be found that no new phase was produced. No pyrochlore-type $Pr_2Zr_2O_7$ and $SrZrO_7$, which have poor oxygen ionic conductivity even at high temperatures and result in producing a high ohmic resistance between electrode and electrolyte, were formed between the optimized composition of the sample (20% Sr content) with YSZ electrolyte. For LSF20, there was a trace amount of YFe_2O_4 between PSF20 and YSZ after reaction at 1000°C [14]. Pr^{3+} replaced La^{3+} at A-site can hamper the reaction between the cathode and electrolyte. The result was same with the report of Sakaki et al. [5]. It can be explained that $Pr_2Zr_2O_7$ was suppressed because the wide solid solution range of Pr/Zr appears in $Pr_2Zr_2O_7$, which transforms to a disordered fluorite structure at higher temperature [27]. Compared to the XRD patterns of PSF20 (omitted in Fig. 11) in Fig. 2a and cubic $Y_{0.15}Zr_{0.85}O_{1.93}$ (Card No. 30-1468), the PSF20 unit cell volume and the cubic YSZ unit cell volume all slightly expanded. The volume expansion can be attributed to the Zr and Y ions diffusion from YSZ into perovskite lattice of PSF20. And the Pr and/or Sr ions diffused into the lattice of YSZ. The diffusion would result in cell expansion because the ionic radii of Y^{3+} (0.9 Å) and Zr^{4+} (0.72 Å) are larger than the Fe^{3+} (0.645 Å) and Fe^{4+} (0.585 Å), and the ionic radii of Pr and Sr are larger than those of Y and Zr [8,28]. $Pr_{0.8}Sr_{0.2}FeO_3$ exhibits superior chemical stability with YSZ electrolyte.

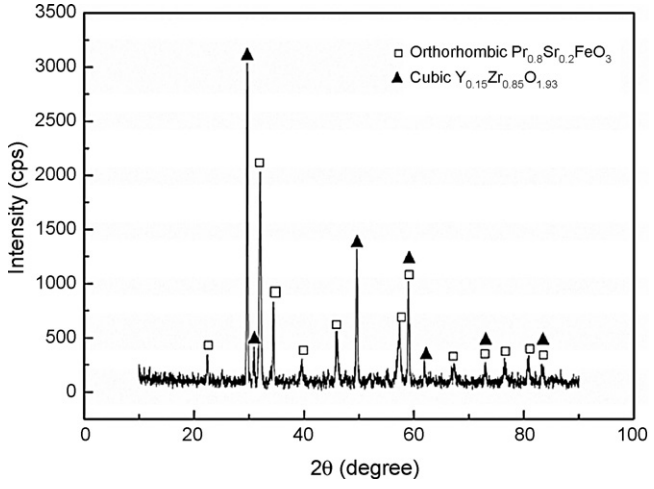

Fig. 11. The XRD pattern of the PSF20–YSZ mixture annealed at 1200 °C for 6 h and then heat-treated at 800 °C for 100 h.

Next steps for this study are to study the performance of PSF–YSZ and PSF–GDC composite cathodes and the long-term stability of the PSF20 on YSZ electrolyte under SOFC operating conditions.

4. Conclusion

The physical properties and electrochemical characteristics of Sr-doped praseodymium ferrite were investigated. All the samples of $Pr_{1-x}Sr_xFeO_3$ (x = 0–0.5) were single phase. The X-ray diffraction results showed that $Pr_{1-x}Sr_xFeO_3$ (x = 0.1–0.3) exhibit the orthorhombic $PrFeO_3$ structure and took the cubic structure when x = 0.4 and 0.5. The unit cell volume decreased with increasing strontium content due to smaller size of the Fe^{4+} (0.585 Å) as compared with that of Fe^{3+} (0.645 Å) in B-site. It has well thermal expansion compatibility with YSZ electrolyte when $x \leq 0.3$. The electrical conductivities of $Pr_{1-x}Sr_xFeO_3$ were all higher than 100 S cm^{-1} when x = 0.3–0.5. The $Pr_{0.8}Sr_{0.2}FeO_3$ a maximum conductivity of 300 S cm^{-1} at 550 °C and $Pr_{0.8}Sr_{0.2}FeO_3$ is 78 S cm^{-1} at 800 °C. There are lower R_p values of the samples which x = 0.1–0.3 compared with that of $La_{0.8}Sr_{0.2}MnO_3$ and the lowest R_p value achieved for $Pr_{0.8}Sr_{0.2}FeO_3$ (0.2038 Ω cm^2). The value of I_0 for $Pr_{0.8}Sr_{0.2}FeO_3$ at 800 °C is 123.6 mA cm^{-2}, which is higher than that of $La_{0.8}Sr_{0.2}MnO_3$. Compared with the $La_{0.8}Sr_{0.2}FeO_3$ cathode, $Pr_{0.8}Sr_{0.2}FeO_3$ exhibits superior chemical stability with YSZ electrolyte. The $Pr_{1-x}Sr_xFeO_3$ materials can be used as a new cathode material for SOFC.

Acknowledgements

The project is financially supported by the National Natural Science Foundation of China (No. 90510006) and by 863 National Project (2003 AA302440).

References

[1] C. Lu, T.Z. Sholklapper, C.P. Jacobson, S.J. Viso, L.C. De Jonghe, J. Electrochem. Soc. 153 (2006) A1115–A1119.

[2] F. Riza, Ch. Ftikos, F. Tietz, W. Fischer, J. Eur. Ceram. Soc. 21 (2001) 1769–1773.

[3] T.J. Armstrong, J.G. Rich, J. Electrochem. Soc. 153 (2006) A515–A520.

[4] S. Tanasescu, N.D. Totir, D.I. Marchidan, Solid State Ionics 119 (1999) 311–315.

[5] Y. Sakaki, Y. Takeda, A. Kato, N. Imanishi, O. Yamamoto, M. Hattori, M. Iio, Solid State Ionics 118 (1999) 187–194.

[6] E. Koep, D.S. Mebane, R. Das, C. Compson, M. Liu, Electrochem. Solid-State Lett. 8 (2005) A592–A595.

[7] M.J. Jørgensen, S. Primdahl, C. Bagger, M. Mogensen, Solid State Ionics 139 (2001) 1–11.

[8] H. Ullmann, N. Trofimenko, F. Tietz, D. Stöver, A. Ahmad-Khanlou, Solid State Ionics 138 (2000) 79–90.

[9] J.-H. Wan, J.-Q. Yan, J.B. Goodenough, J. Electrochem. Soc. 152 (2005) A1511–A1515.

[10] H.Y. Tu, Y. Takeda, N. Imanishi, O. Yamamoto, Solid State Ionics 17 (1999) 277–281.

[11] S.P. Simner, J.F. Bonnett, N.L. Canfield, K.D. Meinhardt, J. Power Sources 113 (2003) 1–10.

[12] G.Ch. Kostogloudis, Ch. Ftikos, J. Eur. Ceram. Soc. 18 (1998) 1707–1710.

[13] H.W. Brinks, H. Fjellvåg, A. Kjekshus, B.C. Hauback, Structure and magnetism of $Pr_{1-x}Sr_xFeO_{3-\sigma}$, J. Solid State Chem. 150 (2000) 149–233.

[14] S.P. Simner, J.P. Shelton, M.D. Anderson, J.W. Stevenson, Solid State Ionics 161 (2003) 11–18.

[15] K. Knizek, Z. Jirak, E. Pollert, F. Zounova, J. Solid State Chem. 100 (1992) 292–300.

[16] E.V. Bongio, H. Black, F.C. Raszewski, D. Edwards, C.J. Mcconville, R. Vasantha, W. Amarakoon, J. Electroceram. 14 (2005) 193–198.

[17] D. Kek, P. Panjan, E. Wanzenberg, J. Eur. Ceram. Soc. 21 (2001) 1861–1865.

[18] S.P. Simner, J.F. Bonnett, N.L. Canfield, K.D. Meinhardt, V.L. Sprenkle, J.W. Stevenson, Electrochem. Solid-state Lett. 5 (2002) A173–A175.

[19] E. Perry Murray, S.A. Barnett, Solid State Ionics 143 (2001) 265–273.

[20] Y. Matsuzaki, I. Yasuda, Solid State Ionics 126 (1999) 307–313.

[21] E.P. Murray, T. Tsai, S.A. Barnet, Solid State Ionics 110 (1998) 235–243.

[22] M.J. JØrgensen, S. Primdahl, M. Mogensen, Electrochim. Acta 44 (1999) 4195–4201.

[23] A.V. Virkar, J. Chen, C.W. Tanner, J.-W. Kim, Solid State Ionics 131 (2000) 189–198.

[24] X. Huang, J. Liu, Z. Lu, W. Liu, L. Pei, T. He, Z. Liu, W. Su, Solid State Ionics 130 (2000) 195–201.

[25] T. Ishihara, T. Kudo, H. Matsuda, Y. Takita, J. Electrochem. Soc. 142 (1995) 1519–1524.

[26] S. Kim, S. Wang, X. Chen, Y.L. Yang, N. Wu, A. Ignatiev, A.J. Jacobson, B. Abeles, J. Electrochem. Soc. 147 (2000) 2398–2406.

[27] L. Qiu, T. Ichikawa, A. Hirano, N. Imanishi, Y. Takeda, Solid State Ionics 158 (2003) 55–65.

[28] M.-F. Hsu, L.-J. Wu, J.-M. Wu, Y.-H. Shiu, K.-F. Lin, Electrochem. Solid-State Lett. 9 (2006) A193–A195.